A Strained Silicon Cold Electron Bolometer using Shottky Contacts

T. L. R. Brien,[1, a)] P. A. R. Ade,[1] P. S. Barry,[1] D. V. Morozov,[1] M. J. Prest,[2] R. V. Sudiwala,[1] T. E. Whall,[2] and P. D. Mauskopf[1, 3]

[1)] *School of Physics & Astronomy, Cardiff University, Queen's Buildings, The Parade, Cardiff, CF24 3AA, United Kingdom*

[2)] *Department of Physics, University of Warwick, Coventry, CV4 7AL, United Kingdom*

[3)] *School of Earth & Space Exploration, Arizona State University, 650 E. Tyler Mall, Tempe, AZ 85287, United States of America*

(Dated: 16 October 2013)

We present a novel type of bolometric detector which utilises Schottky contacts between a superconductor and n^{++} silicon to directly cool the electrons in the absorber. We show that, using these contacts, the electron temperature can be reduced to substantially below that of the phonon-lattice. Finally, we show that a preliminary detector, using a twin-slot antenna to couple 150 GHz radiation, operating at a phonon-lattice temperature of 350 mK is currently able to achieve a noise equivalent power in the area of 10^{-17} W Hz$^{-1/2}$. Further to this, we show that, with simple changes to the detector, we can improve this by at least an order of magnitude. We also discuss routes to improved performance of the detector.

PACS numbers: 07.57.Kp, 85.25.Pb, 63.20.Kp, 84.30.Le
Keywords: Bolometers, Superconducting Devices, Infrared Radiation, Noise, Phonon-Electron Interactions, Electrical Amplifiers

I. INTRODUCTION

The concept of using tunnelling junctions to cool electrons to temperatures below that of the phonons has been developed over the last twenty years[1–4]. The operation principle behind this type of device is that the hottest electrons are extracted and replaced by electrons from a biasing current. This occurs, as at low temperature (typically below 1 K), the electrons are thermally isolated from the phonons and thus this process causes the temperature of the electrons to be decreased. A typical working example of this concept is the Normal Metal-Insulator-Superconductor (NIS) structure, where the tunnelling junction consists of insulator (often an oxide layer).

FIG. 1 shows a typical NIS structure. Without any external bias, the Fermi-energy of the normal metal lies in the middle of the superconducting gap and all the subgap states in the superconductor are filled. This means that, in this unbiased state, there can be no movement of electrons from the normal metal to the superconductor. However, if a biasing voltage, V, is applied across the device, such that the energy levels in the normal metal are raised sufficiently ($eV \geq \Delta$) to correspond to vacant states above the superconductor's gap, electrons are now able to move out of the normal metal. By carefully choosing the biasing voltage, we can select only the most energetic (hottest) electrons. The cooling power of these devices can be increased by using a symmetric structure with the volume to be cooled (the normal metal) in the centre and tunnelling contacts on both sides (SINIS)[2].

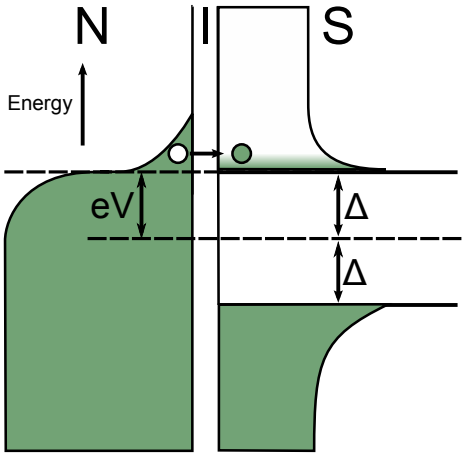

FIG. 1. Energy bands for a biased NIS structure. In order for electrons to tunnel from the normal metal (left) into the superconductor (right), we require that $eV > \Delta$, where V is the voltage across the structure due to the bias and Δ is half the superconducting gap.

These devices have been shown to be able to reduce electron temperature from 300 mK to below 100 mK[3].

A similar structure, SSmS, exists where the normal metal is replaced by a doped semiconductor and the insulator replaced by a Schottky contact formed between the semiconductor and the superconductor[5]. These devices have the advantage of decreased electron-phonon coupling compared to the SINIS type of device[6].

The Cold Electron Bolometer (CEB) utilises this type of device by adding an additional route for energy to couple in to the central volume (the detector's absorber). Optical power is able to raise the energy of the electrons in the absorber and thus allow them to tunnel out (providing their total energy is sufficient). If we apply a bias-

[a)] Electronic mail: tom.brien@astro.cf.ac.uk

ing voltage just less than the required amount (2Δ), then there will be no current across the device. If, however, the additional energy from photons further raises the energy of the electrons to greater than 2Δ, then electrons will be able to tunnel and current will flow. There are two obvious advantages of this detection regime. Firstly, it should be extremely sensitive; by carefully choosing the biasing voltage, the CEB can be setup in such a way that only a small amount of optical power is required for tunnelling. Secondly, because the cooling (thermal resetting) of the bolometer is carried out directly by electron extraction (as opposed to the long, weak, thermal links required by many of today's most sensitive bolometers[7–9]) the thermal time constant associated with the CEB is governed by the tunnelling time. This can be as low as 10 ns[10], whereas other types of detector have response times of the order of 1 ms[11].

II. DEVICE DESIGN

The Strained Silicon CEB, studied in this work, consists of three elements: Firstly, the silicon substrate, which has a straining layer; upon which is 30 nm mesa of n^{++} doped silicon ($N_D = 4 \times 10^{19}$ cm^{-3}); finally, the top layer is made of aluminium. This final layer forms both the contacts to the doped silicon absorber, as well as containing the etched twin slot antenna.

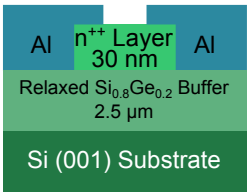

(a)

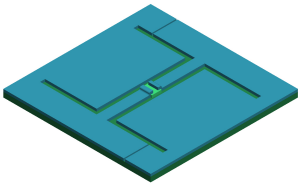

(b)

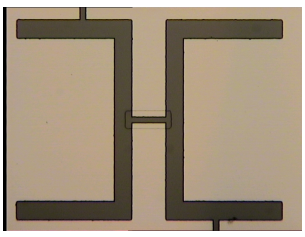

(c)

FIG. 2. (a) Cross-sectional view of CEB structure. (b) 3-dimensional model of a single pixel SiCEB. A small island absorber of n^{++} doped silicon (light green) sits on top of the strained silicon substrate (dark green); the top layer of aluminium (blue) forms both the antenna structure and the contacts to the absorber; the small slots, which can be seen to the edges of the device, ensure that DC continuity is broken within the aluminium. (c) Optical image of 150 GHz CEB.

The mesa structure has an area of 38 µm × 14 µm and, along the twin slot antenna within the aluminium, has been created using photo lithography.

III. THEORY

Rather than relying on conventional thermal links to cool the detector, the CEB has the ability to self-cool after a detection event and indeed, due to this electron cooling, the CEB is also able to operate at temperatures below the phonon bath temperature (as described in SEC. I). The electrons are cooled by a cooling power, P_c, which is given by:

$$P_c = \frac{2}{e^2 R_N} \int_\Delta^\infty \frac{E^2}{\sqrt{E^2 - \Delta^2}} \times \left[f\left(E - E_{in}, T_e\right) - f\left(E + E_{in}, T_e\right) \right] \mathrm{d}E, \tag{1}$$

where $f(E,T)$ is the Fermi distribution, for electrons at temperature T_e, and E_{in} is the energy input into the electron system by the biasing voltage (eV) and the optical radiation (E_O), given by:

$$E_{in} = E_O + \frac{eV}{2}, \tag{2}$$

In addition to this cooling power, the electrons are also heated by the weak thermal link to the phonons. This heating term, P_{e-ph}, is given by:

$$P_{e-ph} = \Sigma\Omega \left(T_{ph}^\beta - T_e^\beta \right), \tag{3}$$

where Σ is a material constant that has been measured[6] to be 2×10^7 W K^{-6} m^{-3}; Ω is the volume of the bolometer's absorber; T_{ph} and T_e are the phonon and electron temperatures respectively and the power β has been found[6] to be 6. From this we can define a thermal conductance, G, from the phonons to the electrons as:

$$G = \frac{\mathrm{d}P}{\mathrm{d}T_{ph}} = 6\Sigma\Omega T_{ph}^5. \tag{4}$$

As this transfer of energy from the phonons to the electrons will lead to a shot noise contribution to the electrical noise, we can define a fundamental limit to the noise equivalent power (NEP) of the CEB in terms of this contribution. This limit will be[12]:

$$NEP_{phonon}^2 = 4k_B T_{ph}^2 G. \tag{5}$$

The other dominant limiting factor to the NEP will be the photon noise. This term is well known to be:

$$NEP_{photon}^2 = 2h\nu P, \tag{6}$$

where ν and P are the frequency and power of the incident radiation respectively.

Finally, the current, I, across the device due to a biasing voltage is given by:

$$I = \frac{1}{eR_N} \int_\Delta^\infty \frac{E}{\sqrt{E^2 - \Delta^2}} \times \left[f\left(E - \frac{eV}{2}, T_e\right) - f\left(E + \frac{eV}{2}, T_e\right) \right] \mathrm{d}E. \tag{7}$$

IV. EXPERIMENTAL PROCEDURE

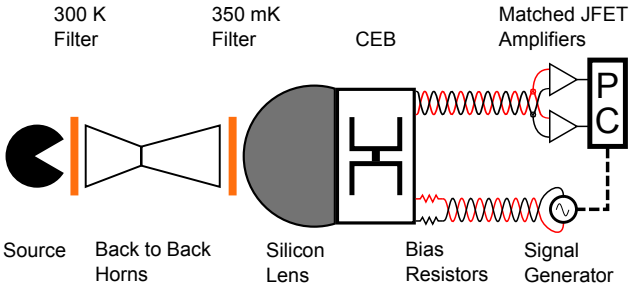

FIG. 3. Experimental setup, radiation is focussed onto the detector chip via a pair of back-to-back horns and a silicon lens. Optical filters are placed before and after the horns and have the effect of limiting the radiation seen by the detector to an upper limit of 300 GHz. The detector is biased via a simple voltage generator and biasing resistors. The voltage output of the detector is split and sent to two JFET based amplifiers (each with an input referred noise of 2 nV $\mathrm{Hz}^{-1/2}$) and the output of these is correlated to achieve a final input refereed noise of 300 pV $\mathrm{Hz}^{-1/2}$.

Testing of the Silicon CEB was performed in two liquid helium cryostats, one for dark testing and one for optically loaded tests. Both systems utilised a further helium sorption cooler and the readout electronics were equivalent. A schematic of the testing setup, when optically loaded, is shown in FIG. 3. Radiation, visible through a window in the outer cryostat shield, was fed in to a pair of back-to-back horns, the beam from this horn pair was then focussed on to the detector's antenna by a hemispherical silicon lens.

The detector was biased using a simple arrangement of a differential voltage source and a pair of biasing resistors. The voltage output of the detector was fed into two matched JFET differential amplifiers (based upon the Texas Instruments' INA103KU chip) each of which had an input referred noise of 2 nV $\mathrm{Hz}^{-1/2}$. The output of each of these amplifiers was then passed to a computer which cross-correlated the signal in realtime and resulted in a final input referred noise, after averaging, of 300 pV $\mathrm{Hz}^{-1/2}$ for the readout system.

For optical testing two different sources were used: firstly, the general laboratory surroundings (≈ 300 K) and secondly, liquid nitrogen (77 K).

V. RESULTS

The Silicon CEB has been tested in a number of scenarios, both dark and optically loaded. Dark measurements mainly consist of IV characterisation. A typical low temperature IV curve for a SiCEB is shown by the blue (least linear) curve in FIG. 4. It is clear that, for voltages below approximately 350 μV, there is negligible current flow. As the voltage increases beyond this the current begins to rise. From this and the earlier description (SEC. I) we can see that 350 μV corresponds to 2Δ.

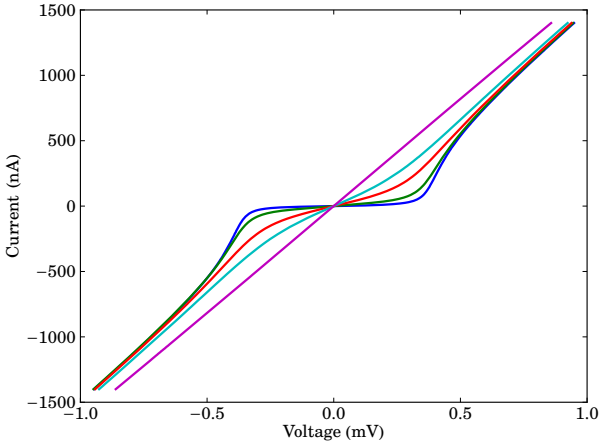

FIG. 4. IV characterisation of a SiCEB at various phonon temperatures. It can be seen that the Dynes parameter tends towards 1 as the temperature increases towards the critical temperature (1.2 K). Blue (outer most) to magenta (inner most): $T_{ph} = 250$ mK, 500 mK, 700 mK, 900 mK and 1.2 K.

The behaviour of the IV characteristics has also been observed as a function of bath temperature. When considering all data sets FIG. 4, it is clear to see that the IV curve tends to the linear as the temperature approaches the critical temperature of aluminium (1.2 K), which results in the Dynes parameter increasing towards unity.

The response to two different optical sources is shown in FIG. 5. This is similar to that of FIG. 4; as in both

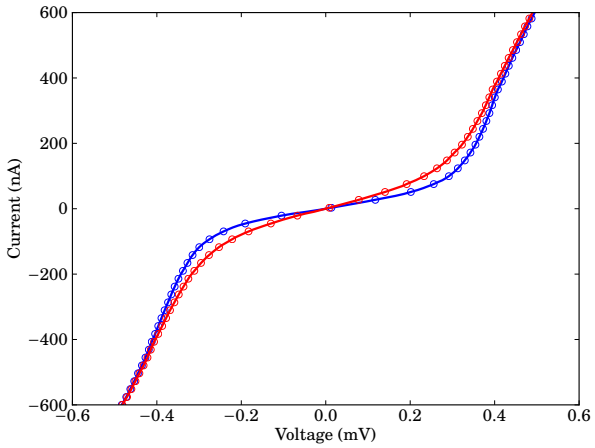

FIG. 5. IV characteristics and model fit. Blue - 77 K source. Red - 300 K source. There is a clear shift of the IV towards the linear as the incident power is increased. Solid line - Model fit based on T_e fitting in EQN. 7. Circles - Heavily reduced experimental data.

cases the energy of the electrons in the absorber is increased. The process of optically loading the detector creates a higher response (on a per-power basis) compared to increasing T_{ph} since the coupling of the energy is more efficient than in the case of heat flowing from the phonons to the electrons via the weak link between these two systems.

By taking each voltage point from the IV curve and using EQN. 7 we can calculate the temperature of the electrons, we can then produce a model to fit these data by finding the value of T_e which yields the correct corresponding current. This has been performed for IV curves measured when the detector is looking at each source in turn. This model, shown as the solid lines in FIG. 5, shows that a high quality fit can be achieved based on this algorithm in both cases. The electron temperatures found from this fit were 570 mK and 660 mK at zero bias for the 77 K and 300 K illuminations. The increase from the phonon temperature of 350 mK is accounted for by the incident power heating the electrons. At a bias corresponding to a voltage of 2Δ across the detector, the minimum electron temperatures achieved for the two illumination levels were 300 mK and 490 mK. From this, it is possible to calculate the difference in the power absorbed between the two states. We found this to be 1.49 pW.

The responsivity can be calculated from the difference in the IV curves from FIG. 5 and the absorbed power (1.5 pW). This is measured to have a maxima of 4.3×10^7 V W^{-1}, when the voltage across the device is equal to 2Δ. FIG. 6 shows the calculated noise equivalent power in the described scenario. This is dominated by the photon noise (EQN. 6). From FIG. 6 we see that the NEP is 2×10^{-17} W Hz$^{-1/2}$.

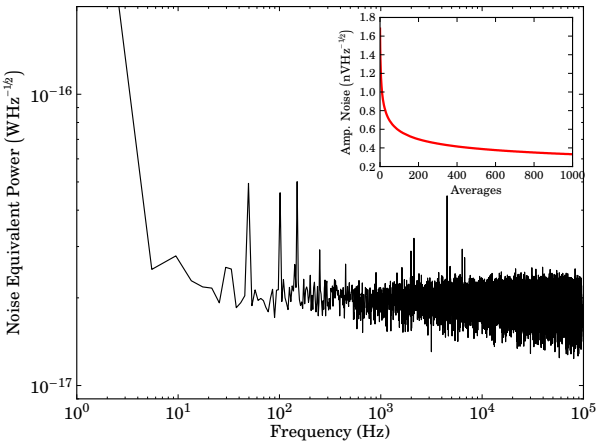

FIG. 6. Noise equivalent power for a SiCEB, operating at optimum bias ($V = 2\Delta$) with a source 1.5 pW above the background. Inset: Reduction in amplifier noise with averaging for two JFET amplifiers operating in cross-correlated mode.

The speed of the detector can be found from the roll-off in the white noise level from the photon noise; this, however, could not be measured in this work (as seen in FIG. 6) due to being faster than the bandwidth of the amplifier (100 kHz). From this, we deduce that the time-constant of this detector is less than 1 µs.

From the use of EQN. 5 and the details of the detector's physical characteristics (given in SEC. II), we can compute that the limit on the electrical (dark) noise equivalent power, from the electron-phonon interaction, is 8.25×10^{-18} W Hz$^{-1/2}$. Furthermore if the area of the absorber and the phonon temperature were each to be lowered by a factor of two (both are viable), this limit would become 3×10^{-19} W Hz$^{-1/2}$.

VI. CONCLUSION

We have demonstrated a new type of detector that utilises direct electron cooling via Schottky tunnelling contacts between aluminium and strained silicon. We have shown that this detector has a noise equivalent power of 2×10^{-17} W Hz$^{-1/2}$ (limited by photon noise from 1.5 pW loading) and a limiting electrical noise equivalent power, at 350 mK, of 8.25×10^{-18} W Hz$^{-1/2}$. The time constant of this detector has been determined to be less than 1 µs, which, along with the NEP, compares extremely favourably to other detector types.

[1] M. Nahum, T. M. Eiles, and J. M. Martinis, Applied Physics Letters **65**, 3123 (1994).
[2] M. M. Leivo, J. P. Pekola, and D. V. Averin, Applied Physics Letters **68**, 1996 (1996).
[3] J. P. Pekola, T. T. Heikkilä, A. M. Savin, J. T. Flyktman, F. Giazotto, and F. W. J. Hekking, Phys. Rev. Lett. **92**, 056804 (2004).
[4] J. Pekola, Nature **435**, 289 (2005).
[5] A. M. Savin, M. Prunnila, P. P. Kivinen, J. P. Pekola, J. Ahopelto, and A. J. Manninen, Applied Physics Letters **79**, 1471 (2001).
[6] M. J. Prest, J. T. Muhonen, M. Prunnila, D. Gunnarsson, V. A. Shah, J. S. Richardson-Bullock, A. Dobbie, M. Myronov, R. J. H. Morris, T. E. Whall, E. H. C. Parker, and D. R. Leadley, Applied Physics Letters **99**, 251908 (2011).
[7] M. D. Audley, G. de Lange, J.-R. Gao, P. Khosropanah, M. Ridder, L. Ferrari, W. M. Laauwen, M. Ranjan, P. D. Mauskopf, D. Morozov, and N. A. Trappe, in *Proc. SPIE 8452, Millimeter, Submillimeter, and Far-Infrared Detectors and Instrumentation for Astronomy VI* (2012) pp. 84520B–84520B–12.
[8] W. S. Holland, D. Bintley, E. L. Chapin, and A. Chrysostomou, Monthly Notices of the Royal Astronomical Society **430**, 2513 (2013).
[9] P. D. Mauskopf, J. J. Bock, H. D. Castillo, W. L. Holzapfel, and A. E. Lange, Appl. Opt. **36**, 765 (1997).
[10] L. Kuzmin, in *12th International Conference on Infrared and Millimeter Waves* (2004) pp. 239–240.
[11] B. D. Jackson, P. A. J. De Korte, J. Van der Kuur, P. Mauskopf, J. Beyer, M. Bruijn, A. Cros, J. Gao, D. Griffin, R. Den Hartog, M. Kiviranta, G. De Lange, B. van Leeuwen, C. Macculi, L. Ravera, N. Trappe, H. Van Weers, and S. Withington, Terahertz Science and Technology, IEEE Transactions on **2**, 12 (2012).
[12] S. H. Moseley, J. C. Mather, and D. McCammon, Journal of Applied Physics **56**, 1257 (1984).